Scientia Horticulturae 318 (2023) 112087

Contents lists available at ScienceDirect

Scientia Horticulturae

journal homepage: www.elsevier.com/locate/scihorti

Early detection of grapevine graft incompatibility: Insights into translocated and virus-induced incompatibility

Sara Tedesco [a,b,c], Patricia Irisarri [d,e], Margarida Teixeira Santos [f], Pedro Fevereiro [a,c], Ana Pina [d,e,*,1], Friedrich Kragler [b,*,1]

[a] Plant Cell Biotechnology Laboratory, Instituto de Tecnologia Química e Biológica António Xavier (ITQB, Green-it Unit), 2780-157 Oeiras, Portugal
[b] Department 2, Max Planck Institut für Molekulare Pflanzenphysiologie, 14476 Potsdam-Golm, Germany
[c] InnovPlantProtect CoLab, 7350-999 Elvas, Portugal
[d] Departamento de Ciencia Vegetal, Centro de Investigación y Tecnología Agroalimentaria de Aragón (CITA), 50059 Zaragoza, Spain
[e] Instituto Agroalimentario de Aragón-IA2 (CITA-Universidad de Zaragoza), 50013 Zaragoza, Spain
[f] Instituto Nacional de Investigação Agrária e Veterinária (INIAV), 2780-159 Oeiras, Portugal

ARTICLE INFO

Keywords:
Grapevine
GRSPaV
Histology
Graft incompatibility
In vitro culture
Syrah

ABSTRACT

In vineyards to control phylloxera (*Daktulosphaira vitifolia* Ficth) attacks in *Vitis vinifera* L., heterografted vines are planted using American vines hybrids as rootstocks. However, graft incompatibilities can affect grape yield and plant longevity. Thus, to identify early graft incompatibility factors, we established *in vitro* micrografting protocols coupled with histology and histochemistry analysis in grapevine graft combinations of known compatibility behavior. The histochemical characterization of the graft union revealed irregular cell arrangement, slower vascular differentiation, persistence of the necrotic layer, accumulation of starch, and lower differentiation of phloem cells in hetero- compared to homografts, indicating the presence of translocated incompatibility symptoms. We highlight the utility of evaluating the graft interface cellular arrangement and starch content via calcofluor and I_2KI staining, respectively, as allowed to identify the graft combinations with lower graft success. Wounded and grafted Syrah plantlets pointed out an impaired sucrose distribution in these plants and levels of Grapevine Rupestris Stem Pitting associated Virus (GRSPaV) infections correlated with graft (un)-success in two Syrah clones micrografted onto 110-Ritcher rootstock. Furthermore, silencing GRSPaV before grafting increased graft success rates. We propose that grapevine graft incompatibility is mainly a virus-induced phenomenon that can arise even in certified plants.

1. Introduction

Grafting of plants is used since ancient times in horticulture and orchards as a tool for plant propagation and improvement. It is used for the intensification of production in more than 70 woody crops (Warschefsky et al., 2016) and more than 80% of the vineyards all over the world are currently composed of *Vitis vinifera* scions grafted onto Phylloxera-resistant American hybrids rootstocks (Ollat et al., 2016). Graft incompatibility can result in propagation losses affecting the ultimate performance of a grafted plant and grafting also constitutes an entry point for dissemination of pathogens and diseases (Tedesco et al., 2022). Graft incompatibility is defined as the failure to form a successful graft union between two plant parts when all other requirements, such as technique, timing, phytosanitary and environmental conditions are satisfied (Assunção et al., 2019). Graft incompatibility can manifest in short-term graft failure resulting in early death or long-term decline of vineyards both causing economic losses to nurseries and grapevine growers. Despite centuries of research on interactions between scions and rootstocks, the graft-induced alteration of plant traits, and the occurrence of graft-transmissible diseases, these are still poorly understood (Tedesco et al., 2022). Clearly, finding a reliable way to predict graft incompatibilities would be tremendously useful in grapevine rootstock breeding programs, although it is a real challenge (Pina et al., 2017). Traditionally, graft incompatibility in fruit trees has been

* Corresponding authors.
E-mail addresses: s.tedesco@iplantprotect.pt (S. Tedesco), pirisarri@aragon.es (P. Irisarri), margarida.santos@iniav.pt (M. Teixeira Santos), psalema@itqb.unl.pt (P. Fevereiro), apina@aragon.es (A. Pina), kragler@mpimp-golm.mpg.de (F. Kragler).
[1] Both authors contributed equally to this work.

https://doi.org/10.1016/j.scienta.2023.112087
Received 25 February 2023; Received in revised form 15 April 2023; Accepted 17 April 2023
Available online 28 April 2023

classified as translocated or localized (Mosse, 1962). Translocated incompatibility is found associated as in peach/plum graft combinations with the accumulation of starch above the union, phloem degeneration, and early defects on growth (Zarrouk et al., 2006). Conversely, localized incompatibility is characterized as in apricots (*Prunus armeniaca* L.) when grafted on other *Prunus* species, by poor vascular connectivity leading to mechanical weakness and subsequent breakdown at the graft union (Errea et al., 2001). Another classification includes graft failure due to virus and/or phytoplasma presence, named virus-induced graft incompatibility as reported for orange trees, sweet cherry, walnut, apple trees (Mosse, 1962), and grapevines (Rowhani et al., 2017). Although grapevine is known to be the host of over 80 distinct virus species (Fuchs, 2020), just a few of them are object of specific control regulations within the European Union ("Commission Implementing Regulation (EU) 2019/2072 of 28 November 2019"). Hence, it is unsure whether the use of certified vines is sufficient to exclude the occurrence of virus-induced graft incompatibility problems. For instance, among the viruses excluded from the certification schemes, Grapevine Rupestris Stem Pitting associated Virus (GRSPaV) is one of the most ubiquitous and variable viruses in grapevine. GRSPaV is suspected to be involved in different diseases, such as in 'Rupestris stem pitting' and 'Vein necrosis' (inducing symptoms in *V. rupestris* and Ritcher-110 (110R), respectively), as well as in 'Syrah decline' (Rowhani et al., 2017), although a definitive proof for its involvement is lacking.

In the last decades, *in vitro* micrografting has been implemented as an experimental system for early graft incompatibility studies to bypass several *in vivo* constraints such as minimizing environmental variability and biotic interferences (Assunção et al., 2021; Cui et al., 2019). Localized incompatibility was studied *in vitro* by histological analysis of the graft union in apricot grafts (Errea et al., 2001; Pina et al., 2012) and in pear grafts demonstrating that an early detection of incompatible unions is possible (Espen et al., 2005). Furthermore, a number of histochemical studies implicated the role of specific cellular compounds in the scion–rootstock interaction, such as cellulose, lignin, phenols, and starch in trees (Errea et al., 2001; Pina et al., 2012; Pina and Errea, 2008). Although *in vitro* grafting was used to identify incompatible interactions of rootstocks with virus-infected scions of Cabernet Franc (Cui et al., 2019), few histochemical studies have been performed on grapevine during graft union development (D'Khili et al., 1995). In the present study, we assessed the suitability of *in vitro* systems as early detection methods for grapevine incompatibility and identified early cellular markers leading to a disturbed graft union formation using certified virus-free homografted (i.e., a graft between two individuals of the same genotype) and heterografted (i.e., a graft between two genotypes) grapevine micrografts, with known graft compatibility response when grafted onto the worldwide used rootstock 110R (*V. berlandieri* x *V. rupestris*).

2. Materials and methods

2.1. Plant material and in vitro growth

Scion branches of certified plants of four *V. vinifera* clones cv. 'Touriga Nacional', clone 21 ISA/PT and clone 112 JBP/PT (TN21 and TN112 respectively) and cv. 'Syrah', ENTAV-INRA/FR clones 383 and 470 (SY383 and SY470 respectively) were collected from the Portuguese National Ampelographic Collection (PRT051) located at Quinta da Almoinha, Dois Portos, Portugal in July 2017. Branches from the rootstock genotype 'Ritcher-110′ (*V. berlandieri* x *V. rupestris*, JBP/PT clone, 110R) were harvested from a mother plant maintained under greenhouse conditions. At the time of collection, the absence of grapevine leafroll-associated virus-1 (GLRaV-1), −2 (GLRaV-2), −3 (GLRaV-3), Arabis mosaic virus (ArMV), Grapevine fanleaf virus (GFLV), and of Grapevine fleck virus (GFkV) was confirmed by enzyme-linked immunosorbent assay (ELISA) by the plant virology laboratory of the National Institute for Agricultural and Veterinary Research (INIAV, Portugal). Nodal segments from all genotypes were disinfected for 15 min in 30% commercial bleach (Domestos® Unilever, Portugal) and rinsed in sterile dH_2O three times. Explants were cultured in tubes containing 1/2-strength macro- and micro-elements of Murashige and Skoog (1962), 1 mL/L vitamins (Galzy, 1969), 30 g/L sucrose, 5 mg/L dithiothreitol, and 7 g/L agarose and were maintained at 24±1 °C and 16/8 h (~40 µmol/m^2/s; light/dark) in an environmentally controlled growth chamber.

2.2. Graft success and phenotypic evaluations

Slit micrografts of TN21/TN21, TN112/TN112, SY383/SY383, SY470/SY470, 110R/110R, TN21/110R, TN112/110R, SY383/110R and SY470/110R, with described compatibility behavior (Assunção et al., 2019; Renault-Spilmont et al., 2005; Tedesco et al., 2020), were performed according to Yildirim et al. (2010). All *in vitro* grafted plants were grown in culture boxes under the same media composition and growth conditions used to propagate the non-grafted plants. Grafts were considered successful when growth of the scion and/or rooting of the rootstock was observed at 49 DAG. At this time point, graft success (%) and the collection of phenotypic parameters including growth of the scion (cm), number of roots, and length of the main root (cm) were recorded. In addition, five successful graft unions per combination were fixed in FAA at 28 and 49 DAG, paraffin-embedded, and sectioned at 10 µm under a rotary microtome (Leica RM2255, Germany) for histochemical analysis.

2.3. Histochemical analysis and quantification

Three biological graft union repetitions per combination and timepoint were stained with 0.07% (w/v) calcofluor in dH_2O (30 s incubation) to stain cellulose in the cell wall (Hughes and McCully, 1975), 0.01% (w/v) acridine orange (30 s incubation) for lignified cell walls (differentiating xylem at the graft junction) (Demarco, 2017; Houtman et al., 2016), phloroglucinol-HCl (10% phloroglucinol in 100% ethanol for 3 min followed by 3 min incubation in 37% HCl) for lignins (Ros Barceló, 1998), I_2KI (2 g of potassium iodide (IK) and 0.2 g of iodine (I) were dissolved in 100 mL of distilled water, 10 min incubation) for starch, and 0.1% (w/v) aniline blue (10 min incubation) for callose deposition (Leszczuk et al., 2019). The samples were viewed under a Leitz Ortholux II fluorescence microscope (Leitz, Wetzal, Germany) with a Leica DC300 camera and the epifluorescence of calcofluor, acridine orange, and aniline blue staining was detected using a BP355–425 excitation filter and a LP460 emission filter. The assignment of phenotypic scores (i.e., A = low, B = intermediate, and C = high) to graft combinations was based on cellular arrangement detected with calcofluor, on grade of vascular differentiation using acridine orange, and on intensity of staining at the necrotic layer separating the two grafting partners using phloroglucinol-HCl. I_2KI stained images were used to quantify the number of starch granules per cell by measuring starch granules and cell numbers in three randomly chosen grids of equal area on the scion and three on the rootstock using Fiji/ImageJ (National Institute of Health, USA, version 1.52p) in three biological repetitions (captured images) per graft combination. The same approach was used to analyze aniline blue stained images to measure the ratio of callose deposition per cell.

2.4. Grapevine rupestris stem pitting associated virus (GRSPaV) detection

The presence of GRSPaV in leaves of non-grafted *in vitro* plant material (SY383, SY470, and 110R) was analysed by quantitative reverse transcription polymerase chain reaction (qRT-PCR). Total RNA from leaves (3 biological replicates/genotype, each being a pool of leaves from 3 plants) was extracted as described (Assunção et al., 2019) and 200 ng of total RNA per sample was used for cDNA synthesis in 20 µl ImProm-II™ Reverse Transcriptase reaction (Promega, Madison, WI,

USA) with a universal poly(T) primer (10 mM) following the manufacturer's instructions. qRT-PCR reactions for each cDNA sample and non-template controls were carried out on a LightCycler 480 system (Roche Diagnostics, Penzberg, Germany) using the published "48 V/49C" universal GRSPaV primers (Lima et al., 2006) and ubiquitin (UBI) primers (forward: AGTAGATGATGACTGGATTGGAGGT, and reverse: GAGTATCAAAACAAAAGCATCG, NCBI accession: XM_002273532.2) as a reference gene for relative quantification. PCR mix contained 10 µl SYBR Green SuperMix (Quanta Biosciences, Gaithersburg, MD, USA), 0.6 µl / primer (10 mM), and 1.25 ng of cDNA in 20 µl reaction volume. All qRT-PCR reactions were run with the following cycle conditions: 5 min at 95 °C, followed by 45 cycles of 95 °C for 10 s, 55 °C for 10 s, and 72 °C for 30 s. Melting curve analysis (up to 97 °C) was performed following amplification using LightCycler® 480 Software Release 1.5.1.62 SP3. Cycle Threshold (Ct) values provided by the software were used to compile the relative expression values (fold change) of the target viral transcript in leaves of SY383 and SY470 following normalization to the control sample (leaves of 110R) and the reference gene (UBI) as described (Pfaffl, 2001).

2.5. Plant monitoring in response to wounding and to sucrose

Micropropagated SY383, SY470, and 110R (3.5 months grown *in vitro*) plants were cut at their shoot base and 3 plants/genotype were placed on a culture box containing fresh media (supplemented with 3% sucrose). 3 culture boxes were prepared per genotype (total of 9 plants/genotype). The plant phenotype after wounding was imaged at least once every 10 days with an Olympus camera (Olympus OM-D EM5 MarkII, Tokyo, Japan) for > 4 months until plant recovered or plant death. Additionally, plantlets of SY383 and SY470 were cut and placed on new culture media supplemented with 3%, 1.5%, and 0% sucrose (9 plants/genotype/treatment). Visual phenotypic response of these plants to the media treatment was documented 1 and 3 months after wounding. 6 homografts of SY383 were also placed on culture media supplemented with 3%, 1.5%, and 0% sucrose and their phenotypic response was monitored at least once every 10 days.

2.6. Viral identification and double-stranded RNA (dsRNA) construction

Total RNA from SY383 and SY470 leaves (pool of 3 plants/genotype) was extracted as previously described (Assunção et al., 2019). 0.1 µg of RNA per sample was used for cDNA synthesis in AMV Reverse Transcriptase (AMV-RT) (Promega, Madison, USA) reaction according to the manufacturer's instructions. RT-PCR reactions were performed using the "48 V/49C" universal GRSPaV primers and the RuBisCO large subunit (rbcL) (forward: GAGTTCCACCCGAAGAAGCA, and reverse: GCTCGATGTGGTAGCATCGT, NCBI Accession: JN114848.1) primers as a positive control. PCR amplifications (40 cycles) were done with 54 °C annealing temperature using DreamTaq DNA Polymerase (Thermo Scientific, Waltham, MA) and supplied reaction mix. PCR amplicons were confirmed by electrophoresis (2% agarose gel) and Midori Green Advance (Nippon Genetics, Düren, Germany) DNA stain. The amplified GRSPaV PCR products in SY383 and SY470 leaves, were gel purified and cloned into Pjet1.2/blunt vector (Thermofisher Scientific, Waltham, MA), transformed into TOP10 *E.coli* and the clones were sequenced (~15 clones / GRSPaV PCR product) and analyzed using BLAST and Clustal W (MEGA software version X). One of the most representative GRSPaV transcript variants found in SY470 was selected to serve as a DNA template for the dsRNA construct producing siRNAs targeting the viral coat protein (CP) sequence. Table S2 lists the oligonucleotides used to produce the DNA template of an antisense RNA with a hairpin (HP) with nick, and of a sense RNA with a tRNA-like structure (TLS) with nick. The HP and TLS motifs were included in the dsRNA construct forming a circular RNA with increased silencing efficacy of ectopically applied dsRNA. Equal amounts of gel-purified sense and antisense cDNA template (4 µg in 50 µl reaction) were *in vitro* transcribed using the T7 RiboMAX Express Large Scale RNA Production System (Promega, Madison, USA) being the reaction carried out at 30 °C overnight in a water bath. The transcribed RNA was treated with Turbo DNA-free™ Kit (Ambion, Life Technologies, Ltd.) and the sense and antisense RNA was precipitated overnight at −20 °C (with 0.1 vol. 3 M sodium acetate and 1 vol. Isopropanol) and resuspended in sterile dH_2O. Finally, the RNA was heated at 92 °C followed by snap-cooling on ice to form dsRNA with hairpins (Burge et al., 2014) prior to application onto the cut grapevine stem surface prepared for grafting and wounding. The predicted (HP and TLS) structures of the GRSPaV dsRNA were done using the Vienna RNA folding predictor (Gruber et al., 2008) and are shown in Fig. S3. dsRNA with *Yellow Fluorescent Protein* (YFP) matching dsRNA sequences and HP and TLS motifs and sterile dNTP mix (10 mM) were used as negative controls.

2.7. dsRNA application and evaluation of GRSPaV silencing in wounded and micrografted grapevines

SY470 and the rootstock 110R plants grown in media supplemented with 1.5% sucrose were selected for the experiment. Wounded, homografted, and heterografted plants were processed as shown in Fig. S2 under a sterile bench. At 49 DAG, graft success rates and the phenotypic parameters were measured as described above, and the wounded, homo- and heterografted plants were collected (pool of technical duplicates) for molecular analysis. In the case of heterografts, scions and rootstocks were detached before collection and all scions from each group were pooled to form one treated and one control sample. RNA extraction and qRT-PCR of these samples were carried out as described above except that, besides UBI primers, also Glyceraldehyde-3-phosphate dehydrogenase (GAPDH) primers (Forward: 5- TTC TCG TTG AGG GCT ATT CC −3, and reverse: 5- CCA CAG ACT TCA TCG GTG ACA −3, NCBI accession: XM_002263109.3) were used as a reference gene for relative quantification. Leaves from 110R collected before the experiment were used as calibrator sample and the value of 45 was attributed in case of no target amplification.

2.8. Data analysis and statistics

Statistical analysis of all data was performed in RStudio (RStudio Team, 2015. RStudio: Integrated Development for R. RStudio, Inc., Boston, MA, USA, http://www.rstudio.com/). Phenotypic parameters (i.e., shoot growth (cm), root number, and length of the main root (cm)) from the phenotypic screenings on micrografts, number of starch granules/cell, and number of callose depositions/cell were analysed by Kruskal–Wallis test and multiple comparisons of treatments in the Rpackage "agricolae" (de Mendiburu, 2020). Data are shown as mean values ± SE (standard error) and significant differences are reported at * $p < 0.05$, ** $p < 0.01$, *** $p < 0.001$. Contingency tables of the phenotypic scores attributed to the level of cellular arrangement, differentiation, and intensity of staining were used as data input to compute the chi-square test of independence and evaluated for a significant association between the graft combinations and the attributed scores. Pearson residuals were extracted using the function chisq.test() and the package corrplot used to visualize and present these results according to Kassambara (Kassambara, 2016). Student's *t*-test was performed to compare the presence of the GRSPaV in each sample in relation to the calibrator sample and the expression levels of the used reference genes. The mean of the $\log_2$ expression levels ± SE is shown.

3. Results

3.1. In vitro graft success is higher in homografts and failed grafted plants display a viral phenotype

The phenotypic assessment of graft success at 49 days after grafting (DAG) revealed that it ranged from 48% to 100% in homografts, and

from 23% to 80% in heterografts (Fig. 1a).

According to the phenotypical evaluation of heterografted plants, TN112/110R had the highest graft success rate under *in vitro* conditions (Fig. 1a), which was unexpected as this combination is considered relatively incompatible (Assunção et al., 2019). Similarly, SY383/110R, known as incompatible (Renault-Spilmont et al., 2005; Tedesco et al., 2020), displayed a higher success than SY470/110R (Fig. 1a). Noteworthy, failed grafts showed a high red coloration phenotype resembling a viral infection (Basso et al., 2017) (Fig. 1b) which was detected already at 28 DAG. Successful grafts often formed a single scion leaf that turned red undergoing senescence before the scion resumed growth appearing asymptomatic (Fig. 1b). According to the phenotypic evaluation at 49 DAG, the shoot growth was not significantly different between the graft combinations or the graft type (i.e., homo- or heterografts). However, heterografted plants with 110R rootstocks formed significantly more and longer roots compared to homografts (Table S1).

3.2. The Syrah clone with higher failure rates displays higher levels of GRSPaV infection

To elucidate whether the lower graft success of SY470/110R compared to SY383/110R (Fig. 1a) could be correlated with GRSPaV infection levels, we measured the presence of viral GRSPaV transcripts by qRT-PCR on 110R, SY383, and SY470 leaf samples of *in vitro* grown plantlets. Implying a relationship between viral presence and low graft success of SY470 heterografts, the GRSPaV transcript measurements revealed a significantly higher viral presence in SY470 compared to SY383 (Fig. 2), whereas GRSPaV transcript levels in the rootstock genotype (110R) were below the detection threshold (Ct > 35).

3.3. Heterograft vascular differentiation proceeds slower than in homograft and the necrotic layer persists at 49 DAG

To identify early cellular marks of an incompatible scion-rootstock interaction, stained graft union sections were scored (i.e., A = low, B = intermediate, C = high) for their spatial cellular arrangement (calcofluor), level of vascular differentiation (acridine orange), and presence of a necrotic layer (Phloroglucinol-HCl). Likewise, significant associations between the anatomical parameters evaluated and the graft

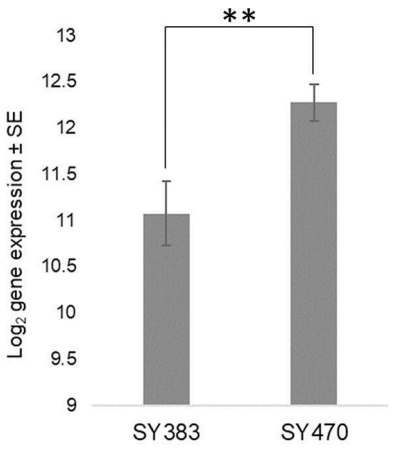

Fig. 2. Relative presence of GRSPaV transcripts in leaves of SY383 and SY470 *in vitro* plantlets detected by qRT-PCR. Mean of $\log_2$ expression levels ± SE of biological and technical replicates are presented. Significant difference was detected at ** $p < 0.01$ by Student's *t*-test ($n = 3$ / graft combination. 1 sample is a pool of 3 plants, 3 technical replicates).

combinations, graft type (homo- or heterograft), and time (28 and 49 DAG) were identified by chi-square test of independence at $p < 0.05$ (Table 1).

At 28 DAG, there was a significant association between the graft combinations and the cellular arrangement (Table 1). Indeed in Fig. 3a, showing examples of calcofluor stained sections used to assess the level of cellular arrangement, it can be noticed that SY470/110R at 28 DAG displayed a low order in the cellular arrangement of its graft union compared to SY383/110R (Fig. 3a).

Indeed, the highest relative contributions in terms of Pearson residuals (Pr) were assigned to SY470/110R for its relatively low cellular arrangement (A score, Pr = 2.858) and, secondarily to SY383/110R for its high cellular arrangement (C score, Pr = 1.792) at 28 DAG (Fig. 3b). Regarding the result obtained with Acridine Orange staining, only homografts showed a significant association to the grade of cellular differentiation between the two times of observation (i.e., 28 and 49 DAG) (Table 1). In contrast to heterografts, homograft unions appeared significantly more differentiated at 49 DAG than at 28 DAG (Fig. 3c,d).

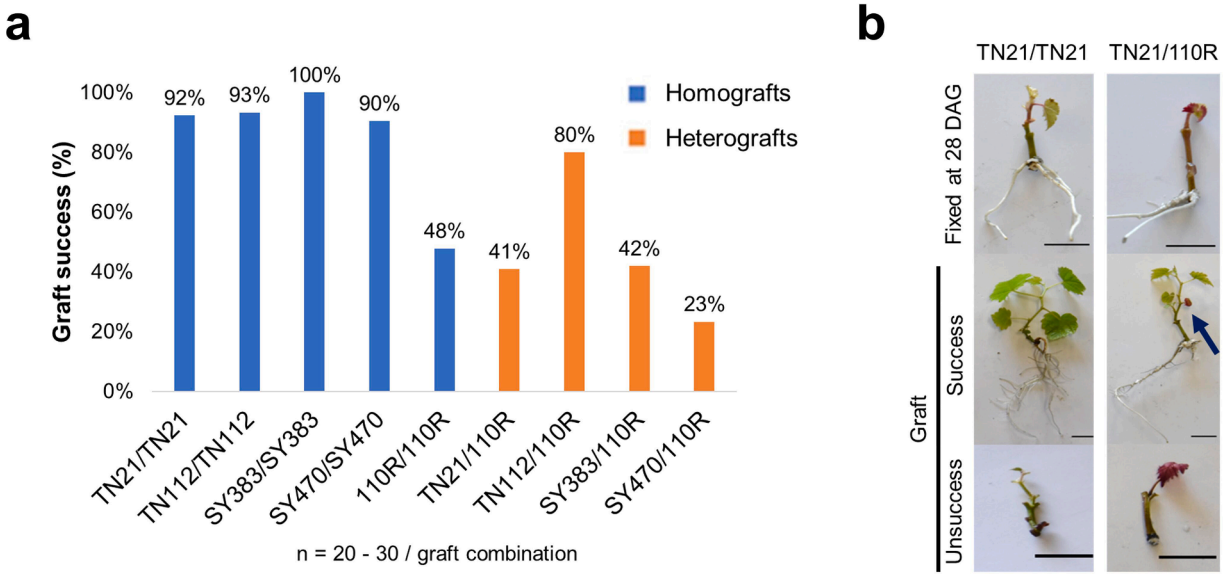

Fig. 1. Graft success rate and examples of detected graft phenotypes. Bar chart of graft success (%) per graft combination at 49 DAG according to regain of root and/or scion growth (**a**). Example images of successful and unsuccessful TN21 homo- and heterografted plants at 49 DAG, and fixed at 28 DAG (**b**). The blue arrow indicates senescence detected at the first leaf. $n = 20 – 30$ / graft combination. Scale bars = 1 cm.

Table 1
Significant associations according to the chi-square test of independence for the qualitative scores attributed at 28 and 49 DAG for the cellular arrangement, cellular differentiation, and intensity of staining in response to the graft combination, graft type, and time. Level of significance indicated by asterisks symbols: *** $p < 0.001$; ** $p < 0.01$, * $p < 0.05$; ns: no-significant difference. $n = 3$ observations per graft combination / time-point / staining.

	Graft combinations		Graft type (homo/heterograft)		Time (28 and 49 DAG)	
Parameter	28 DAG	49 DAG	28 DAG	49 DAG	Homo-	Heterograft
Cell arrangement-*Calcofluor*	29.018 *	ns	ns	ns	ns	ns
Cell differentiation - *Acridine Orange*	ns	ns	ns	ns	6 *	ns
Intensity of staining - *Phloroglucinol HCl*	ns	ns	ns	15.406 ***	ns	7.224 *

The vascular connection of homografts was completed across the graft junction at 49 DAG while the vascular bundles were rarely traversing the heterografted tissues at the same time point. This difference was statistically significant according to Pearson residuals (Fig. 3d) with a low level of differentiation in homografts at 28 DAG (score A, Pr = 0.981 and score C, Pr = −1.414) and with a high level of differentiation at 49 DAG (score C, Pr = 1.414 and score A, Pr = −0.981).

Phloroglucinol-HCL indicates the presence of lignin in interfascicular fibers, and the stained sections of the graft junctions were scored for the presence of a necrotic layer. The results indicated a significant association between staining and the type of graft at 49 DAG and also within the group of heterografts between times (Table 1). Heterografts showed significantly higher lignin fluorescence at the necrotic layer than homografts at 49 DAG, which also significantly increased at 49 when compared to 28 DAG samples (Fig. 3e). Indeed, Pearson residuals showed that the highest contributions were based on the low intensity of lignin staining detected in homografts (score A, Pr = 1.732 and score B, Pr = −1.512). This was different from the high-intensity staining detected in heterografts at 49 DAG (score B, Pr = 1.766 and score A, Pr = −2.023) (Fig. 3f, below). Similarly, a significant increase in staining was observed in heterografts at 49 DAG in comparison to 28 DAG (score A, Pr = −1.283 and score *B* = 1.450; and score A, Pr = 1.229 and score B, Pr = −1.388, respectively) (Fig. 3f, above). Hence, the necrotic layer in heterografts not only persists at 49 DAG, but is even more stained at 49 than at 28 DAG.

3.4. Heterografts scion-rootstock translocation and phloem regeneration is impaired compared to homografts

Presence of starch granules at the graft interfaces revealed by potassium iodide-iodine reaction (I_2KI) staining can be a good indicator of proper sugar distribution in grafted plants. To this end, we measured the average number of starch granules/cell and of callose depositions/cell, as well as the significant differences for each of the graft combination, graft type, tissue (i.e., scion and rootstock), and time at $p < 0.05$, (Table 2). Touriga Nacional homografts were more depleted in starch than 110R and Syrah homografts, being SY383/SY383 the graft combination with higher content of starch at 28 DAG (Table 2). Although TN112/TN112 had the lowest number of starch granules per cell at 28 DAG, a significantly increased starch content was detected in heterografted TN112/110R, while no significant differences were detected between homo- and heterografted TN21 and Syrah cultivars (Table 2).

Interestingly, all heterografted plants were significantly more enriched in starch granules than homografts at both 28 and 49 DAG time points (Fig. 4a; Table 2).

The rootstock was always more enriched in starch than the scion, most likely due to sucrose uptake from the growth medium. Over time, the starch content significantly decreased being higher at 28 DAG than at 49 DAG, indicating an increased sugar consumption along with the healing of the graft union (Table 2, Fig. 4a). As expected, the 110R root genotype contributed to the significant difference seen between homo- or heterografts at 49 DAG. However, TN21/110R vs. TN21/TN21 and SY470/SY470 vs. SY470/110R were the only graft combinations showing a significant difference by 110R roots being always more enriched in starch than when self-grafted (Table 2). Callose levels measured by aniline blue fluorescence did not significantly vary between 28 and 49 DAG but a significant difference was detected between scions as being more enriched in callose than rootstocks and in general, in homografts more callose was detected than in heterografts at both times (Table 2). Particularly, both TN21/TN21 and TN112/TN112 were significantly more enriched in callose than their respective heterografts at 49 DAG (Table 2, Fig. 4b).

3.5. Symptoms of in vitro wounded and grafted plants differ between 110R and Syrah plants

We noticed that non-grafted genotypes formed a red canopy after long-term *in vitro* propagation. Furthermore, all genotypes, when cut (wounded) and transferred to a new culture media for propagation, displayed leaf reddening and senescence followed by either recovery or death (Fig. 5).

A red senescent phenotype was already noticed in both Syrah clones one week after cutting, and both started to recover at 55 – 60 days after cutting (DAC). Symptoms in 110R appeared later (at 18 – 21 DAC) and lasted longer, up to 100 DAC, followed by either plant recovery or plant death, being plant death more frequent (Fig. 5).

To verify that the red leaf color change is due to the overproduction of anthocyanins depending on sugar availability, we monitored the phenotype of SY383 and SY470 after one and three months of transfer to 3%, 1.5%, and 0% sucrose media. The red color phenotype was enhanced in the presence of higher sucrose indicating that the plants responded differently to sucrose availability (Fig. S1a). The red color phenotype also resembled the phenotype of unsuccessful heterografted plants (compare Fig. 1b with Fig. 5 and S1a). Notably, SY383/SY383 transferred on 3%, 1.5%, and 0% sucrose media indicated that graft success was depending on sucrose. Red color changes in homografts became visible at 9 DAG when grown on 3% sucrose but not when grown on sucrose-free medium where they could be successfully grafted (Fig. S1b).

3.6. Heterografted plants treated with GRSPaV silencing RNA display higher graft success rates

To find evidence that GRSPaV is involved in the detected lower graft compatibility of Syrah, we silenced GRSPaV transcripts by ectopically applying GRSPaV siRNA-inducing dsRNA (Fig. S2). Here we expect that the presence of dsRNA targeting GRSPaV rescues the incompatibility phenotype. Indeed, graft success rates increased from 67% and 80% to 100% for both hetero- and homografted plants, respectively, at 49 DAG treated with GRSPaV dsRNA (Table 3).

However, no significant difference was detected in the phenotypic analysis at 49 DAG between dsRNA-treated and control samples of wounded, homo-, and heterografted Syrah plants (Table 3). To test whether the GRSPaV dsRNA construct was efficient in silencing GRSPaV, we performed qRT-PCR assays on viral CP mRNA (i.e., the target of the used silencing dsRNA construct) on samples from control and treated plants (Fig. 6). Again, no significant difference was observed at 49 DAG between the treated and control groups of wounded, homo-, and heterografted plants at $p < 0.05$ (Fig. 6) which indicates that 7

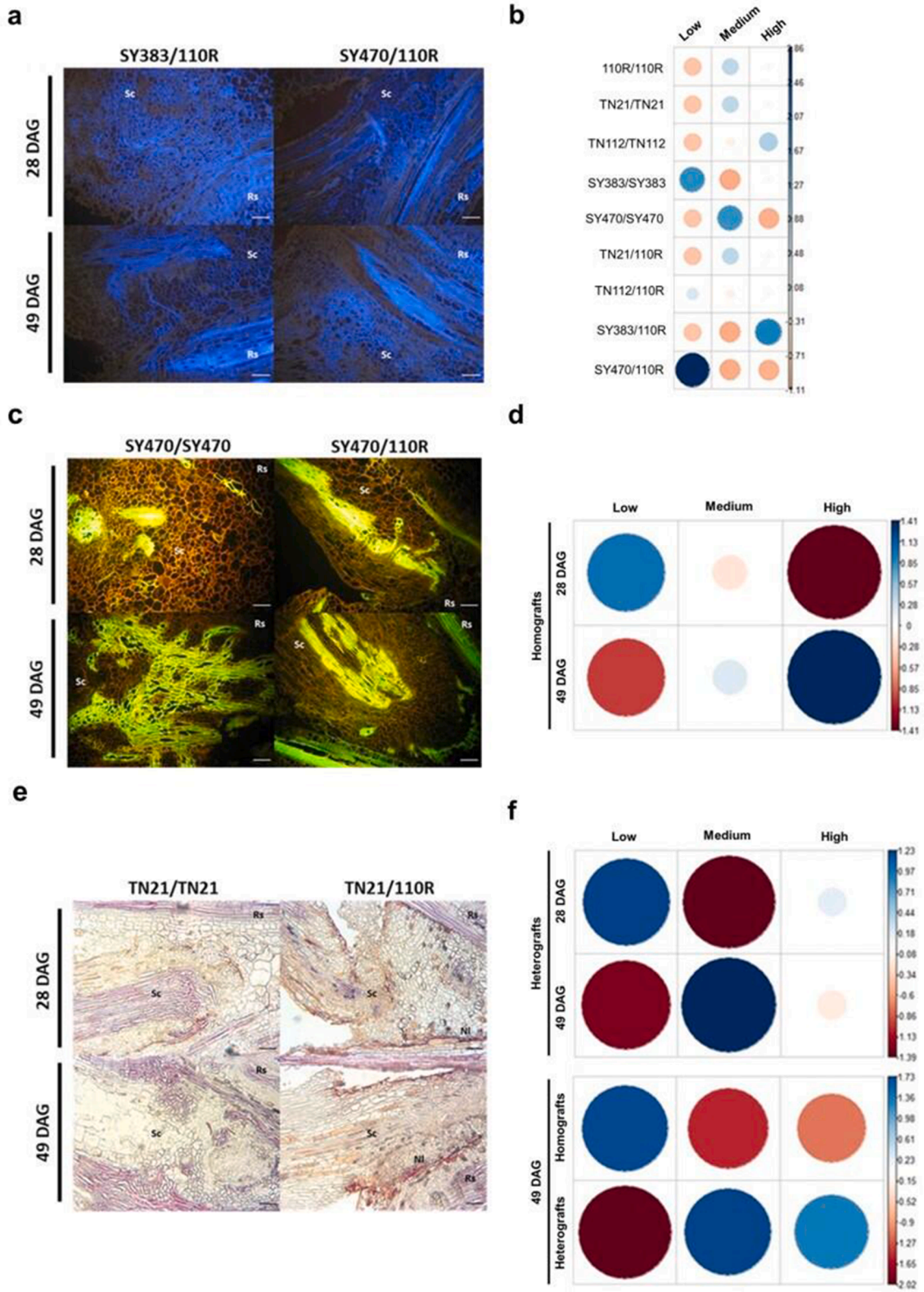

Fig. 3. Histochemical staining of the graft unions at 28 and 49 DAG, and Pearson residuals of the significant associations identified (Table 1) according to the chi-square test of independence at $p < 0.05$. Example micrographs of calcofluor stained sections of SY383/110R and SY470/110R (**a**). Pearson residuals of the cellular arrangements of graft combinations (low, medium, and high arrangement) at 28 DAG (**b**). Acridine orange-stained sections of SY470 homo- and heterografts (**c**), Pearson residuals of the homograft cellular differentiation (low, medium, and high differentiation) between times (**d**). Phloroglucinol-HCl stained sections of TN21 homo- and heterografts (**e**), Pearson residuals for the intensity of the staining at the necrotic layer (low, medium, and high staining) between times, and between homo- and heterografts at 49 DAG (**f**). Positive residuals are shown in blue and negative in red colors. The size of the circles and color intensities are proportional to the value of Pearson residuals. Scion (Sc), Rootstock (Rs), Necrotic layer (Nl). Scale bar = 100 μm.

Table 2
Average number of starch granules per cell, and callose deposition per cell (± SE) at 28 and 49 DAG, per graft combination, graft type, tissue, and time. Significant differences according to Kruskal–Wallis test are indicated by asterisks symbols *** $p < 0.001$; ** $p < 0.01$, * $p < 0.05$. Different letters indicate significant differences. ns: no significant difference. $n = 18$ observations / graft combination / time-point.

		I_2KI - *starch/cell*		*Aniline Blue - callose/cell*	
		28 DAG	49 DAG	28 DAG	49 DAG
Graft combination	***Effect***	***	***	*	*
	110R/110R	81.6 ± 1.6 ab	82.2 ± 1.2 ab	90.1 ± 0.3 ab	77.6 ± 0.3 abcd
	TN21/TN21	45.8 ± 2.0 bc	52.3 ± 0.2 b	67.0 ± 0.3 ab	96.6 ± 0.2 a
	TN112/ TN112	21.3 ± 0.1 c	49.1 ± 0.1 b	72.7 ± 0.1 ab	90.0 ± 0.3 ab
	SY383/ SY383	101.9 ± 1.8 a	55.4 ± 0.4 b	80.7 ± 0.3 ab	93.1 ± 0.2 ab
	SY470/ SY470	87.3 ± 2.0 ab	53.6 ± 0.4 b	105.2 ± 0.2 a	85.1 ± 0.3 abc
	TN21/110R	70.9 ± 1.1 ab	101.0 ± 2.5 a	73.3 ± 0.2 ab	61.1 ± 0.2 cd
	TN112/ 110R	91.2 ± 1.2 a	80.9 ± 1.4 ab	73.0 ± 0.2 ab	53.5 ± 0.1 d
	SY383/ 110R	92.5 ± 2.3 a	88.4 ± 3.3 ab	52.2 ± 0.1 b	67.3 ± 0.1 bcd
	SY470/ 110R	93.4 ± 2.2 a	97.8 ± 2.4 a	65.2 ± 0.2 ab	70.1 ± 0.4 abcd
Graft type	***Effect***	**	***	*	***
	Homograft	66.3 ± 1.8 b	59.5 ± 0.7 b	80.6 ± 0.2 a	88.5 ± 0.2 a
	Heterograft	87.0 ± 1.9 a	91.6 ± 2.5 a	65.6 ± 0.2 b	63.1 ± 0.2 b
Tissue	***Effect***	**	***	***	***
	Scion	66.7 ± 1.5 b	61.4 ± 1.4 b	91.1 ± 0.2 a	94.1 ± 0.3 a
	Rootstock	86.8 ± 2.1 a	90.3 ± 2.3 a	51.6 ± 0.2 b	57.7 ± 0.2 b
Time	***Effect***	***		***ns***	
	28 DAG	174.7 ± 1.9 a		146.7 ± 0.2	
	49 DAG	124.8 ± 2.0 b		153.2 ± 0.2	

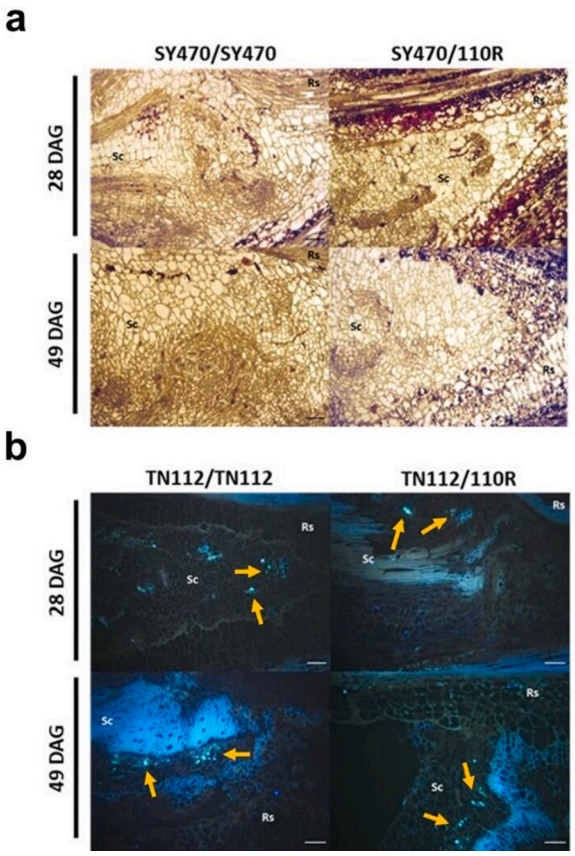

Fig. 4. Starch granules and callose deposition at the graft interface revealed by I_2KI staining in the homo- and heterografts formed by SY470 (**a**) and for aniline blue staining of callose in the homo- and heterografts formed by TN112 (**b**). Scion (*Sc*), Rootstock (Rs), yellow arrows indicate callose deposition signals. Scale bar = 100 μm.

weeks after dsRNA incubation GRSPaV silencing recovered. However, GRSPaV silenced heterografted rootstocks from GRSPaV-free plants (no GRSPaV detected in 110R) showed increased viral transcripts (close to being statistically significant with p-value = 0.1172) compared to the control treatment (Fig. 6), which may indicate that the virus moved from scions to virus-free 110R rootstocks and that a hypersensitive response resulting in early graft failure was delayed or diminished.

4. Discussion

The assessment of graft success indicated that, as expected homografts performed better than heterografts, although TN112 and SY383 performed better than TN21 and SY470 when grafted onto 110R rootstock which is not in agreement with other studies (Assunção et al., 2019; Renault-Spilmont et al., 2005). SY383/110R displayed lower graft success than SY470/110R under field conditions (Tedesco et al., 2020) and leaves of SY383/110R (from plants belonging to the same bulk of cuttings) have higher GRSPaV infection levels than SY470/110R (RNAseq data not shown). Surprisingly, in this *in vitro* micrografted grapevine study most heterograft failures showed typical symptoms of viral infections (Fig. 1b). Regardless of the well-known differences between *in vivo* and *in vitro* grafting systems, we asked whether the found discrepancy regarding *in vitro* and in field graft success rates could be explained by GRSPaV presence in these plants. Indeed, by qRT-PCR we confirmed that the Syrah clone showing less graft success when combined with 110R showed higher GRSPaV transcripts levels both under field and *in vitro* (Fig. 2) conditions. Conversely, GRSPaV was barely or not detectable in the rootstock genotype (110R). To explore the early cellular sign(s) of graft union development in grapevine, we evaluated morphological and histological development in different scion-rootstocks combinations at 28 and 49 DAG. Calcofluor staining revealed a significant association between the graft combinations and their cellular arrangement. Here, the low cellular arrangement found in SY470/110R graft unions correlates with its lower graft success rate (Table 1, Figs. 1a and 3a,b). In a similar line, irregular cell wall thickening and bent cell walls / collapsed cells were observed by calcofluor fluorescence in incompatible *Prunus* grafts (Errea et al., 2001; Pina et al., 2012) and in *callus* tissue from *V. vinifera* grafts infected by both Grapevine leafroll-associated virus-1 (GLRaV-1) and Grapevine virus A (GVA) (Cui et al., 2019). Acridine Orange labeling experiments (Zhang et al., 2017), reveal the progression of vascular differentiation from 28 to 49 DAG across the graft unions. This analysis indicated that in homografts the formation of new vascular bundles crosses the scion and rootstock interface whereas in heterografts the vascular differentiation was significantly delayed (Fig. 3c,d), which was also described in other studies on apple (Richardson et al., 1996), tomato (Frey et al., 2020), and pear/quince graft formations (Espen et al., 2005). The necrotic layer is suggested to be a prerequisite to the formation of continuous secondary plasmodesmata between cells of both grafting partners and to disappear at the moment of *callus* formation in homografts although, in incompatible grafts, its presence seems to hinter full vascular formation between the grafting partners (Pina et al., 2017). Here we show, using Phloroglucinol-HCl staining of the graft junction, that the necrotic layer not only persists longer (compared to homografts) but also increases in heterografted grapevines over time (Table 1, Fig. 3e,f).

Observation of I_2KI stained sections revealed that while starch

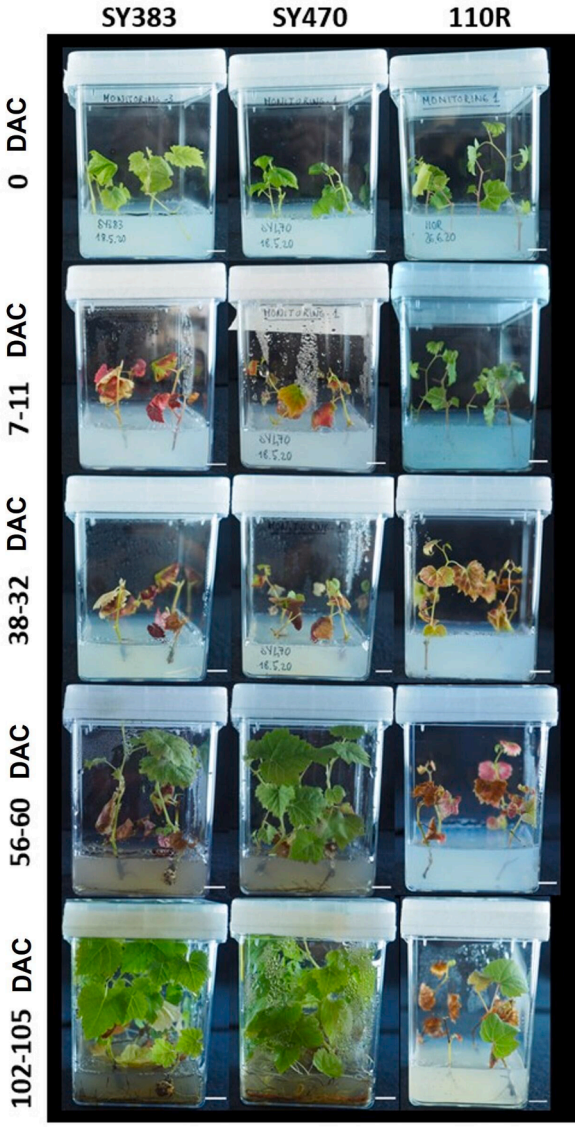

Fig. 5. Recovery after wounding of non-grafted plants. Images taken from propagated SY383, SY470, and 110R plantlets on new culture media supplemented with 3% sucrose from 0 days after cutting (DAC) to 105 DAC. 1 culture box containing 3 plants/genotype is shown, $n = 9$ / graft combination, scale bar = 1 cm.

content decreased over time in homografts, suggesting that starch granules dissolve with the formation of the graft union, the same did not happen in heterografts (Table 2, Fig. 4a). Furthermore, the only genotypes that at 49 DAG were statistically more enriched in starch when grafted onto 110R rather than with themselves (i.e., SY470 and TN21), were also the genotypes showing lower graft success when heterografted, which suggests a negative correlation between graft success and the starch granules content. This might indicate that grapevine graft failures could be a consequence of a reduced sugar translocation between the grafting partners, as it was previously suggested not only for grapevines (Bouquet, 1980) but also in other species (Moing et al., 1987; Schöning and Kollmann, 1997; Zarrouk et al., 2006). One of the first observable processes of sieve elements (SEs) formation is an increase in callose that is deposited in platelet around SEs plasmodesmata (Lucas et al., 2013). Results from the quantification of callose deposition highlighted that phloem regeneration is impaired in heterografts compared to homografts and that the effect is stronger in Touriga Nacional (Table 2, Fig. 4b). It is widely known that auxin and cytokinins

Table 3
Graft success rate and average of roots number, length of the main root (cm), and shoot growth (cm) at 49 DAG per wounded, homo- (SY470/SY470), and heterografts (SY470/110R) treated with GRSPaV dsRNA (Treated) and with dNTPs or *YFP* dsRNA (Control) ± SE. ns: non-significant differences according to Kruskal–Wallis and Mann-Whitney Wilcoxon Tests.

Group	N	Graft Success (%)	Roots number	Main root length (cm)	Shoot growth (cm)
Wounded Control	12	NA	1.4 ± 0.5	2.7 ± 0.9	1.9 ± 0.3
Wounded Treated	12	NA	1.2 ± 0.3	3.1 ± 1	2.3 ± 0.4
Effect			ns	ns	ns
Homografts Control	10	80%	1.0 ± 0.3	3.1 ± 1.0	2.1 ± 0.5
Homografts Treated	10	100%	1.5 ± 0.7	1.4 ± 0.5	1.7 ± 0.3
Effect			ns	ns	ns
Heterografts Control	6	67%	0.8 ± 0.3	3.1 ± 1.3	0.2 ± 0.1
Heterografts Treated	4*	100%	1.5 ± 0.5	2.4 ± 1.1	0.6 ± 0.4
Effect			ns	ns	ns

NA: no available data.
* Two Treated Heterografts were excluded from the analysis as contaminated. Nevertheless, they were already sprouted (graft successful) when contaminated.

concur in phloem development (Lucas et al., 2013) and might offer an explanation for the observed impairment of phloem regeneration as described for *A. thaliana* graft junctions (Serivichyaswat et al., 2022). Furthermore, viruses are known to lead to a degradation of young phloem cells (Esau, 1948) and severe changes in vascular arrangement (Ruiz-Medrano et al., 2007), thus might also be implicated. Hence, more studies should pay attention to the presence of viruses, the phloem tissue differentiation process, and the molecules transferred via phloem in grafted grapevines.

In addition, we have provided evidence that plants phenotypically responded to wounding, thereby displaying a similar but milder phenotype compared to failing heterografted unions (Fig. 5). The presence of symptoms on non-grafted plants once more suggests that grapevine graft incompatibility might be related to viral infection processes. Possibly, latent viral infections in scion genotypes might manifest upon stresses such as grafting and even wounding. For instance, GRSPaV is frequently found in vines affected by “Syrah decline” (Lima et al., 2006) and symptoms were already reported on own-rooted grapevines in Chilean and Argentinian phylloxera-free vineyards (Renault-Spilmont et al., 2010). Furthermore, the detected phenotypic response of wounded and grafted grapevines to different sucrose concentrations in the media (Fig. S1) pointed out a possibly impaired carbon translocation via phloem occurring in these plants. Similar to sugar allocation mutants limited in symplasmic connectivity (Provencher et al., 2001), graft incompatibility is often found associated with the reddening of leaves earlier at the end of the growing season than compatible combinations (Bouquet, 1980; Zarrouk et al., 2006). In grapevines, leaves reddening was explained as an insufficient connection between the rootstock and the scion (Bahar and Korkutal, 2010) and is also reported as a typical symptom in grapevine viral infections, where viruses are known to lead to soluble sugar accumulation in the leaves and deficiency in translocation of these sugars to sink tissues or grape berries (Basso et al., 2017). Certainly, more studies are needed to clarify how and to which extent the phloem function of wounded, grafted, and especially heterografted grapevines is impaired, and how this relates to viruses.

To find evidence for GRSPaV playing a role in Syrah/110R graft incompatibility, we have applied (before grafting) a dsRNA to transiently silence GRSPaV. As anticipated, graft success rates in both homo- and heterografts were successfully rescued (Table 3), supporting the notion that graft incompatibility in grapevine is a virus-induced

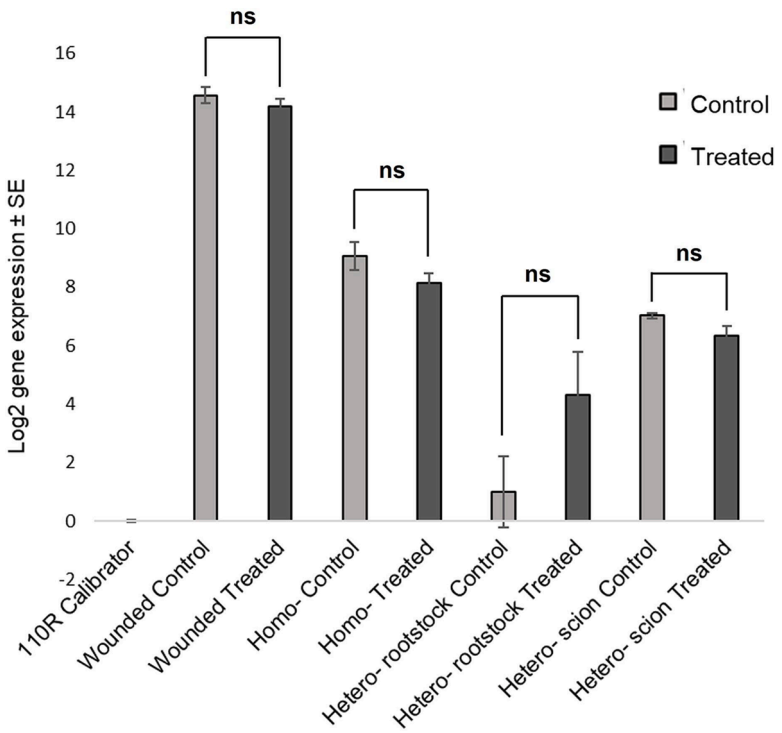

Fig. 6. Relative presence of GRSPaV transcripts in control (not-silenced) and treated (silenced) wounded, homo-, and heterografted SY470 by qRT-PCR. Mean of the log2 expression levels ± SE of biological and technical replicates is presented. $n = 12$ for wounded, $n = 10$ for homografted, $n = 3$ for rootstock and $n = 2$ for scions of heterografted plants / treatment. ns: non-significant difference according to Student's *t*-test ($p < 0.05$).

phenomenon. However, no significant difference in virus presence could be established 7 weeks after dsRNA application (Fig. 6), most probably due to both the low number of plants tested and the long time after incubation selected for the qRT-PCR analysis. Indeed, a great concern of this approach is the well-known recovery of viruses after transient silencing (Das and Sherif, 2020), so nanoparticle based-delivery dsRNA techniques were developed to provide viral protection for longer times (up to 20 days post-treatment compared to the 5-day protection generated by naked dsRNAs) (Mitter et al., 2017). Nevertheless, the putative indication (at 88% of confidence level) that more viral transcripts translocated scion-to-rootstock in GRSPaV silenced heterografts (Fig. 6), seems to support the notion that incompatibility in grapevines is due to the rootstock hypersensitivity to scion-derived viruses (Rowhani et al., 2017; Tedesco et al., 2022). Hence, it could be speculated that the hypersensitive response of the rootstock tissue not only limits the spread of the virus but also prevents the formation of a proper vascular connection, which manifests in the translocated graft incompatibility that we have shown in this work. Certainly, more experimental studies are needed to confirm that the presence of GRSPaV causes the observed changes in Syrah/110R graft compatibility. Despite this, translocated incompatibility symptoms in grapevine heterografts were demonstrated, as well as the utility of *in vitro* techniques (particularly of I_2KI starch and calcofluor cellulose stains) to early screen compatible and incompatible grapevine grafting partners. Furthermore, we have exemplified how dsRNA technology and micrografting may be used to test the involvement of a virus in grapevine graft incompatibility. We encourage its use to support investigations of causal relationships in graft incompatibility studies that aim to find practical solutions to preserve our grapevine germplasm and minimize the incompatibility problems seen by nurseries and growers. Perhaps, similar to what we have shown under *in vitro* micrografting conditions, the use of RNAi-mediated gene silencing of virus on *in vivo* grafted plants might be a useful strategy to improve the growth of incompatible germplasms.

Author contributions

AP, ST, PF, and FK designed the experiments. PF provided the plant material and the micropropagation methods together with MTS who also performed the viral tests by ELISA. ST collected, processed the samples, and analyzed the data. AP and PI supervised the histochemistry methods and analysis. FK supervised the viral silencing experiment and designed the dsRNA constructs. ST and AP wrote the manuscript in collaboration with FK. All authors read, revised, and approved the manuscript.

Data availability statement

The authors confirm that all the experimental data are available and accessible via the main text and/or the supplementary information.

Declaration of Competing Interest

The authors declare that they have no known competing financial interests or personal relationships that could have appeared to influence the work reported in this paper.

Data availability

All the experimental data are available and accessible via the main text and/or the supplementary information

Acknowledgments

This research was supported by internal funds provided to FK from the Max Planck Society, Germany, and by the Fundação para a Ciência e Tecnologia (FCT), Portugal for the Ph.D. grant with the reference PD/BD/128399/2017 and COVID/BD/151639/2021. The authors acknowledge the research unit GREEN-it "Bioresources for

Sustainability" (UID/Multi/04551/2013) and the Gobierno de Aragón-European Social Fund, European Union (Grupo Consolidado A12). The authors thank the National Institute for Agricultural and Veterinary Research (INIAV-Dois Portos) for the provision of the plant material, and Teresa Valdiviesso and Cândida Sofia Trindade (INIAV- Oeiras) for the use of the histology facility. We acknowledge Margarida Basaloco for the reference genes primer design, and Cindy Hauptvogel and Saurabh Gupta in the Kragler laboratory for help in monitoring plants under different sucrose concentrations and analysing RNAseq data for the presence of viral sequences, respectively.

Supplementary materials

Supplementary material associated with this article can be found, in the online version, at doi:10.1016/j.scienta.2023.112087.

References

Assunção, M., Santos, C., Brazão, J., Eiras-Dias, J.E., Fevereiro, P., 2019. Understanding the molecular mechanisms underlying graft success in grapevine. BMC Plant Biol. 19, 1–17. https://doi.org/10.1186/s12870-019-1967-8.

Assunção, M., Tedesco, S., Fevereiro, P., 2021. Molecular Aspects of Grafting in Woody Plants. In: Wiley, J., Sons, L. (Eds.), Annual Plant Reviews Online. Wiley, pp. 87–126. https://doi.org/10.1002/9781119312994.apr0751.

Bahar, E., Korkutal, I., 2010. Using magnetic resonance imaging technique (MRI) to investigate graft connection and its relation to reddening discoloration in grape leaves. JFAE 8 (3&4), 293–297.

Basso, M.F., Fajardo, T.V.M., Saldarelli, P., 2017. Grapevine virus diseases:economic impact and current advances in viral prospection and management. Rev. Bras. Frutic. 39 https://doi.org/10.1590/0100-29452017411.

Bouquet, A., 1980. Differences observed in the graft compatibility between some cultivars of Muscadine grape (Vitis rotundifolia Michx.) and European grape (Vitis vinifera L. cv. Cabernet Sauvignon). Vitis 19, 99–104.

Burge, R.G., Martinez-Yamout, M.A., Dyson, H.J., Wright, P.E., 2014. Structural characterization of interactions between the double-stranded RNA-binding zinc finger protein JAZ and nucleic acids. Biochemistry 53, 1495–1510. https://doi.org/10.1021/bi401675h.

Commission Implementing Regulation (EU), 28 November 2019. Annex IV, Part C available on-line: https://eur-lex.europa.eu/legal-content/EN/TXT/. uri=CELEX/3A32019R2072-lang1=EN-from=PT-lang3=EN-lang2=EN=_csrf=cfae366d-e206-4155-9.

Cui, Z.H., Agüero, C.B., Wang, Q.C., Walker, M.A., 2019. Validation of micrografting to identify incompatible interactions of rootstocks with virus-infected scions of Cabernet Franc. Aust. J. Grape Wine Res. 25, 268–275. https://doi.org/10.1111/ajgw.12385.

Das, P.R., Sherif, S.M., 2020. Application of Exogenous dsRNAs-induced RNAi in Agriculture: challenges and Triumphs. Front. Plant Sci. 11 https://doi.org/10.3389/fpls.2020.00946.

Demarco, D., 2017. Histochemical Analysis of Plant Secretory Structures. pp. 313–330. 10.1007/978-1-4939-6788-9_24.

de Mendiburu, F., 2020. agricolae: statistical Procedures for Agricultural Research. R package version 1, 3-2.

D'Khili, S.G.B., Michaux-Ferrière, N., 1995. Etude histochimique de 1' incompatibilite au microgreffage et greffage de boutures herbacees chez la vigne. Vitis 34, 135–140.

Errea, P., Garay, L., Antonio Marın, J., 2001. Early detection of graft incompatibility in apricot (*Prunus armeniaca*) using in vitro techniques. Physiol. Plant. 112, 135–141. https://doi.org/10.1016/j.scienta.2006.06.011.

Esau, K., 1948. Some anatomical aspects of plant virus disease problems II. Bot. Rev. 14, 413–449. https://doi.org/10.1007/BF02870116.

Espen, L., Cocucci, M., Sacchi, G.A., 2005. Differentiation and functional connection of vascular elements in compatible and incompatible pear/quince internode micrografts. Tree Physiol. 25, 1419–1425. https://doi.org/10.1093/treephys/25.11.1419.

Frey, C., Acebes, J.L., Encina, A., Álvarez, R., 2020. Histological changes associated with the graft union development in tomato. Plants 9, 1–13. https://doi.org/10.3390/plants9111479.

Fuchs, M., 2020. Grapevine viruses: a multitude of diverse species with simple but overall poorly adopted management solutions in the vineyard. J. Plant Pathol. 102, 643–653. https://doi.org/10.1007/s42161-020-00579-2.

Galzy, R., 1969. Galzy, R. Remarques sur la croissance de Vitis rupestris cultivée in vitro sur différents milieux nutritifs. Vitis 8, 191–205.

Gruber, A.R., Lorenz, R., Bernhart, S.H., Neuböck, R., Hofacker, I.L., 2008. The Vienna RNA websuite. Nucleic Acids Res. 36, 70–74. https://doi.org/10.1093/nar/gkn188.

Houtman, C.J., Kitin, P., Houtman, J.C.D., Hammel, K.E., Hunt, C.G., 2016. Acridine orange indicates early oxidation of wood cell walls by fungi. PLoS ONE 11, 1–19. https://doi.org/10.1371/journal.pone.0159715.

Hughes, J., McCully, M.E., 1975. The Use of an Optical Brightener in the Study of Plant Structure. Stain Technol. 50, 319–329. https://doi.org/10.3109/10520297509117082.

Kassambara, 2016. A. Chi-Square Test of Independence in R. R tutorial, available on-line: http://www.sthda.com/english/wiki/chi-square-test-of-independence-in-r.

Leszczuk, A., Pieczywek, P.M., Gryta, A., Frąc, M., Zdunek, A., 2019. Immunocytochemical studies on the distribution of arabinogalactan proteins (AGPs) as a response to fungal infection in Malus x domestica fruit. Sci. Rep. 9, 1–14. https://doi.org/10.1038/s41598-019-54022-3.

Lima, M.F., Alkowni, R., Uyemoto, J.K., Golino, D., Osman, F., Rowhani, A., 2006. Molecular analysis of a California strain of Rupestris stem pitting-associated virus isolated from declining Syrah grapevines. Arch. Virol. 151, 1889–1894. https://doi.org/10.1007/s00705-006-0742-y.

Lucas, W.J., Groover, A., Lichtenberger, R., Furuta, K., Yadav, S.R., Helariutta, Y., He, X. Q., Fukuda, H., Kang, J., Brady, S.M., Patrick, J.W., Sperry, J., Yoshida, A., López-Millán, A.F., Grusak, M.A., Kachroo, P., 2013. The Plant Vascular System: evolution, Development and Functions. J. Integr. Plant Biol. 55, 294–388. https://doi.org/10.1111/jipb.12041.

Mitter, N., Worrall, E.A., Robinson, K.E., Li, P., Jain, R.G., Taochy, C., Fletcher, S.J., Carroll, B.J., Lu, G.Q., Xu, Z.P., 2017. Clay nanosheets for topical delivery of RNAi for sustained protection against plant viruses. Nat. Plants 3. https://doi.org/10.1038/nplants.2016.207.

Moing, A., Salesses, G., Saglio, P.H., 1987. Growth and the composition and transport of carbohydrate in compatible and incompatible peach/plum grafts. Tree Physiol 3, 345–354. https://doi.org/10.1093/treephys/3.4.345.

Mosse, B., 1962. Graft-Incompatibility in fruit trees with particular reference to its underlying causes, Technical. Commonwealth Agricultural Bureaux, England, Farnham Royal, Bucks.

Murashige, T., Skoog, F., 1962. A Revised Medium for Rapid Growth and Bio Assays with Tobacco Tissue Cultures. Physiol. Plant. 15, 473–497. https://doi.org/10.1111/j.1399-3054.1962.tb08052.x.

Ollat, N., Bordenave, L., Tandonnet, J.P., Boursiquot, J.M., Marguerit, E., 2016. Grapevine rootstocks: origins and perspectives. Acta Hortic 1136, 11–22. https://doi.org/10.17660/ActaHortic.2016.1136.2.

Pfaffl, M.W., 2001. A new mathematical model for relative quantification in real-time RT-PCR. Nucleic Acids Res 29, 2002–2007. https://doi.org/10.1111/j.1365-2966.2012.21196.x.

Pina, A., Cookson, S.J., Calatayud, A., Trinchera, A., Errea, P., 2017. Physiological and molecular mechanisms underlying graft compatibility. Vegetable Grafting: Principles and Practices. CABI, Wallingford, pp. 132–154. https://doi.org/10.1079/9781780648972.0132.

Pina, A., Errea, P., 2008. Differential induction of phenylalanine ammonia-lyase gene expression in response to in vitro callus unions of *Prunus* spp. J. Plant Physiol. 165, 705–714. https://doi.org/10.1016/j.jplph.2007.05.015.

Pina, A., Errea, P., Martens, H.J., 2012. Graft union formation and cell-to-cell communication via plasmodesmata in compatible and incompatible stem unions of Prunus spp. Sci. Hortic. (Amsterdam). 143, 144–150. https://doi.org/10.1016/j.scienta.2012.06.017.

Provencher, L.M., Miao, L., Sinha, N., Lucas, W.J., 2001. Sucrose Export Defective1 Encodes a Novel Protein Implicated in Chloroplast-to-Nucleus Signaling. Plant Cell 13, 1127–1141. https://doi.org/10.1105/tpc.13.5.1127.

Renault-Spilmont, A.S., Grenan, S., Bousiquot, J.M., 2005. Syrah decline. Progrés Agric. Vitic. 122, 15–16.

Renault-Spilmont, A.S., Moreno, Y., Audeguin, L., 2010. Syrah decline: similar symptoms on own-rooted plants. Prog. Agric. Vitic. 127, 63–67.

Richardson, F.V.M., tSaoir, S.M.A., Harvey, B.M.R., 1996. A study of the graft union in in vitro micrografted apple. Plant Growth Regul 20, 17–23. https://doi.org/10.1007/BF00024052.

Ros Barceló, A., 1998. The generation of H2O2 in the xylem of Zinnia elegans is mediated by an NADPH-oxidase-like enzyme. Planta 207, 207–216. https://doi.org/10.1007/s004250050474.

Rowhani, A., Uyemoto, J.K., Golino, D.A., Daubert, S.D., Al Rwahnih, M., 2017. Viruses Involved in Graft Incompatibility and Decline. Grapevine Viruses: Molecular Biology, Diagnostics and Management. Springer International Publishing, Cham, pp. 289–302. https://doi.org/10.1007/978-3-319-57706-7_13.

Ruiz-Medrano, R., Moya, J.H., Xoconostle-Cázares, B., Lucas, W.J., 2007. Influence of cucumber mosaic virus infection on the mRNA population present in the phloem translocation stream of pumpkin plants. Funct. Plant Biol. 34, 292. https://doi.org/10.1071/FP06300.

Schöning, U., Kollmann, R., 1997. Phloem translocation in regenerating in vitro - heterografts of different compatibility. J. Exp. Bot. 48, 289–295. https://doi.org/10.1093/jxb/48.2.289.

Serivichyaswat, P.T., Bartusch, K., Leso, M., Musseau, C., Iwase, A., Chen, Y., Sugimoto, K., Quint, M., Melnyk, C.W., 2022. High temperature perception in leaves promotes vascular regeneration and graft formation in distant tissues. Development 149. https://doi.org/10.1242/dev.200079.

Tedesco, S., Fevereiro, P., Kragler, F., Pina, A., 2022. Plant grafting and graft incompatibility: a review from the grapevine perspective. Sci. Hortic. (Amsterdam). 299, 111019 https://doi.org/10.1016/j.scienta.2022.111019.

Tedesco, S., Pina, A., Fevereiro, P., Kragler, F., 2020. A Phenotypic Search on Graft Compatibility in Grapevine. Agronomy 10, 706. https://doi.org/10.3390/agronomy10050706.

Warschefsky, E.J., Klein, L.L., Frank, M.H., Chitwood, D.H., Londo, J.P., von Wettberg, E. J.B., Miller, A.J., 2016. Rootstocks: diversity, Domestication, and Impacts on Shoot Phenotypes. Trends Plant Sci 21, 418–437. https://doi.org/10.1016/j.tplants.2015.11.008.

Yildirim, H., Onay, A., Süzerer, V., Tilkat, E., Ozden-Tokatli, Y., Akdemir, H., 2010. Micrografting of almond (Prunus dulcis Mill.) cultivars "Ferragnes" and "Ferraduel.

Sci. Hortic. (Amsterdam). 125, 361–367. https://doi.org/10.1016/j.scienta.2010.04.022.
Zarrouk, O., Gogorcena, Y., Moreno, M.A., Pinochet, J., 2006. Graft compatibility between peach cultivars and Prunus rootstocks. HortScience 41, 1389–1394.
Zhang, M., Lapierre, C., Nouxman, N.L., Nieuwoudt, M.K., Smith, B.G., Chavan, R.R., McArdle, B.H., Harris, P.J., 2017. Location and characterization of lignin in tracheid cell walls of radiata pine (Pinus radiata D. Don) compression woods. Plant Physiol. Biochem. 118, 187–198. https://doi.org/10.1016/j.plaphy.2017.06.012.